The role of the phosphorus BI-BII transition in protein-DNA recognition: the NF-kappaB complex.

K. Wecker, M. C. Bonnet, E. F. Meurs, M. Delepierre

4452–4459 *Nucleic Acids Research, 2002, Vol. 30 No. 20*

The role of the phosphorus BI–BII transition in protein–DNA recognition: the NF-κB complex

K. Wecker, M. C. Bonnet[1], E. F. Meurs[1] and M. Delepierre*

Unité de RMN des Biomolécules, URA 2185 CNRS and [1]Unité de Virologie et d'Immunologie Cellulaire, URA 1930 CNRS, Institut Pasteur, 28 rue du Docteur Roux, 75015 Paris, France

Received June 19, 2002; Revised and Accepted August 14, 2002

ABSTRACT

We examined, by ^{1}H and ^{31}P NMR, the solution structure of a 16 bp non-palindromic DNA fragment (16M2) containing the HIV-1 NF-κB-binding site, in which the sequences flanking the κB site had been mutated. ^{31}P NMR was particularly useful for obtaining structural information on the phosphodiester backbone conformation. Structural features were then compared with those of the two previously studied DNA fragments corresponding, respectively, to the native κB fragment (16N) and a fragment in which mutations have been introduced at the 5′ end of the κB site (16M1). For the mutated 16M2 duplex, NMR data showed that the BI–BII equilibrium, previously reported for the native fragment (16N) at the κB flanking steps, was lost. The role of the BI–BII equilibrium in NF-κB recognition by DNA was then investigated by electrophoretic mobility shift assay. We found that the isolated κB site has the potential to bind efficiently due to the BI–BII equilibrium of the κB flanking sequences.

INTRODUCTION

The NF-κB transcription factor is an important regulator of genetic processes in the immune and inflammatory responses. NF-κB is subverted by a number of viruses, including the human immunodeficiency virus (HIV) (1–3), the etiological agent of acquired immune deficiency syndrome (AIDS), to activate the expression of viral genes, leading to cell death. The nuclear factor NF-κB, originally identified on the basis of its ability to bind an essential control element located in the immunoglobulin κ light chain locus, is the archetypal member of the class of dimeric Rel proteins (p50, p52 and p65). Rel proteins characteristically have a stretch of approximately 300 amino acids called the rel homology domain (RHD), comprising residues responsible for protein–protein interactions, sequence-specific recognition of DNA and nuclear translocation. NF-κB activity is controlled mainly through interactions with inhibitory proteins of the IκB family, including IκBα and IκBβ. IκB proteins contain six or seven 'ankyrin repeats', each 33 amino acids long, which facilitate interaction with NF-κB, masking the nuclear location signal (NLS) of this protein and resulting in its sequestration in the cytosol. The activation of cells by a variety of inflammatory stimuli, including mitogens, cytokines and oxidative stress, induces the phosphorylation of two serines (Ser32 and Ser36), degradation of the IκB proteins (4,5) and the release of active NF-κB, which is then translocated to the nucleus, where it stimulates the transcription of responsive genes. The active nuclear form of NF-κB is a heterodimeric protein formed by two homologous subunits, p50 (NF-κB1) and p65 (Rel A), assembled by means of their RHDs. Each of these constituent subunits is able to bind DNA alone as a homodimer: p50–p50 (6,7) and p65–p65 (8). Two identical 10 bp sequences, the κB motif, within a region of the HIV-1 long terminal repeat (LTR) extending from –80 to –105 with respect to the transcription start site, have been shown to be high affinity binding sites for NF-κB (2). Transcription initiation occurs only if these DNA sequence motifs are occupied by the transcription factor NF-κB.

Five DNA:NF-κB crystal structures have been published for either homodimer with p50, p52 and p65 (6–9) and a p50–p65 heterodimer (10). The p50–p65 heterodimer recognizes κB elements with the consensus sequence 5′-GGG-RNYYYCC-3′ (R, purine; Y, pyrimidine; N, any nucleotide). In the crystal structure, p50 contacts 5 bp at the 5′ end of the DNA motif, whereas p65 contacts the DNA at the 3′ end of the κB motif (10). Overall, these X-ray studies showed that Rel proteins make contacts with DNA in the major groove via loops connecting the various β-strands of the protein. Furthermore, extensive contacts are made with the phosphate backbone of the cognate DNA. In most of these structures, the DNA helix axis curves towards the major groove, consistent with the results of circular mobility shift assay studies (11).

We recently investigated the intrinsic properties that could confer specificity on a κB DNA site, by determining the NMR solution structure of two non-palindromic 16 bp DNA fragments corresponding to the first NF-κB site (12) and to a fragment into which mutations were introduced at the 5′ end of the κB site (duplex 16M1) (13), abolishing NF-κB binding to DNA (1). We aimed to define the molecular basis of DNA recognition by p50 and p65, to determine whether the lack of binding of the mutated sequence was linked to the intrinsic structural properties of the DNA. In these studies, NMR findings were consistent with a BI–BII equilibrium, for several steps in these two duplexes. In the native duplex, 16N, four pyrimidine–purine steps flanking the 10 bp of the κB site and facing each other in pairs are in BI–BII equilibrium (12). For

*To whom correspondence should be addressed. Tel: +33 1 45 68 88 71; Fax: +33 1 45 68 89 29; Email: murield@pasteur.fr

the mutated duplex, 16M1, a significant BII population is observed only for the κB flanking steps facing each other at the 3′ end, namely $C_{13}pA_{14}$–$T_{19}pG_{20}$. A much smaller BII population is observed at the other two CpA steps, $C_{30}pA_{31}$ and C_6pA_7, at the 5′ end that, due to the mutation, no longer face each other (13). Based on the size of the population of BII conformers, two extreme models of this equilibrium were investigated by molecular modeling for these two duplexes. In one, all the phosphodiester backbones were in the BI conformation (BI family), and in the other the four steps $C_{13}pA_{14}$–$T_{19}pG_{20}$ and $C_{30}pA_{31}$–T_2pG_3 for 16N and $C_{13}pA_{14}$–$T_{19}pG_{20}$ and $C_{30}pA_{31}$–T_6pG_5 for 16M1 were in the BII conformation (BII family). Appropriate refinement gives, for the native duplex, a canonical B-DNA conformation for the BI family and a structure in which the DNA is distorted for the BII family. In the BII family, the NF-κB binding site intrinsically curves towards the major groove. The four flanking steps in the BII conformation magnify this curvature and all the base pairs are pulled into the major groove. The 16M1 duplex also reaches equilibrium between two extreme conformations but, as the distribution of BII sites is different from that in the 16N duplex, the intrinsic structural and dynamic properties of this duplex are very different from those of 16N. It was concluded that the native duplex can reach a conformation in which the helix curves in the same direction as observed in the crystal structures of NF-κB:DNA complexes, with a translation of all the κB base pairs towards a larger major groove. The mutated duplex cannot mimic this conformation and develops no more than one kink at its 3′ end.

The DNA sequence of the native duplex 16N seems to be optimal for BI–BII transition. Indeed, the flexibility of pyrimidine–purine and purine–pyrimidine steps in terms of ε and ζ dihedral angle variations have been extensively studied by Richard Lavery and collaborators by molecular modeling (14–17). Calculations have shown that whatever the flanking sequences, the CpA and CpG steps are more malleable than TpA or purine–pyrimidine steps in terms of BI–BII transition (18). It is also easier to create two BII sites facing each other (18,19). In addition, analysis of the effects of the bases neighboring a given dinucleotide step has indicated that the flexibility of a central pyrimidine–purine step is higher in a tract of pyrimidines followed by a tract of purines (YY sequence on the 5′ side and, preferably, also with an RR sequence on the 3′ side).

As mutations in 16M1 occur at the κB site, it was difficult, at this stage, to determine the effect of this BI–BII transition on the interaction with NF-κB. We therefore designed a new sequence (16M2), in which the κB site was kept intact and mutations were introduced in κB flanking steps only (Fig. 1). In this duplex, the T_2pG_3–$C_{30}pA_{31}$ and $A_{14}pG_{15}$–$C_{18}pT_{19}$ steps of the native κB site are replaced by T_2pA_3–$T_{30}pA_{31}$ and $T_{14}pA_{15}$–$T_{18}pA_{19}$, respectively. The structural features of this new sequence were investigated by ^1H and ^{31}P NMR. ^{31}P NMR was particularly useful for probing the conformation of the phosphodiester backbone, due to its very high sensitivity to conformational changes (20–22). The results obtained were then compared with those obtained for the native 16N and the mutated 16M1 duplexes. The NMR data are consistent with the complete loss of BI–BII equilibrium for the κB flanking steps. The effect of this BI–BII transition on NF-κB binding was then inferred from NF-κB:DNA electrophoretic mobility shift assay.

A $C_1\ T_2\ G_3\ \mathbf{G_4}\ \mathbf{G_5}\ \mathbf{G_6}\ \mathbf{A_7}\ \mathbf{C_8}\ \mathbf{T_9}\ \mathbf{T_{10}}\mathbf{T_{11}}\mathbf{C_{12}}\mathbf{C_{13}}A_{14}G_{15}G_{16}$
$G_{32}A_{31}C_{30}\mathbf{C_{29}}\mathbf{C_{28}}\mathbf{C_{27}}\mathbf{T_{26}}\mathbf{G_{25}}\mathbf{A_{24}}\mathbf{A_{23}}\mathbf{A_{22}}\mathbf{G_{21}}\mathbf{G_{20}}T_{19}C_{18}C_{17}$

B $C_1\ T_2\ G_3\ \underline{C_4}\ \underline{T_5}\ \underline{C_6}\ A_7\ C_8\ T_9\ T_{10}T_{11}C_{12}C_{13}A_{14}G_{15}G_{16}$
$G_{32}A_{31}C_{30}\underline{G_{29}}\underline{A_{28}}\underline{G_{27}}T_{26}G_{25}A_{24}A_{23}A_{22}G_{21}G_{20}T_{19}C_{18}C_{17}$

C $C_1\ T_2\ \underline{A_3}\ \mathbf{G_4}\ \mathbf{G_5}\ \mathbf{G_6}\ \mathbf{A_7}\ \mathbf{C_8}\ \mathbf{T_9}\ \mathbf{T_{10}}\mathbf{T_{11}}\mathbf{C_{12}}\mathbf{C_{13}}\underline{T_{14}}\underline{A_{15}}G_{16}$
$G_{32}A_{31}\underline{T_{30}}\mathbf{C_{29}}\mathbf{C_{28}}\mathbf{C_{27}}\mathbf{T_{26}}\mathbf{G_{25}}\mathbf{A_{24}}\mathbf{A_{23}}\mathbf{A_{22}}\mathbf{G_{21}}\mathbf{G_{20}}\underline{A_{19}}\underline{T_{18}}C_{17}$

Figure 1. Sequences of (**A**) 16N, (**B**) 16M1 and (**C**) 16M2, the duplex mutated at the flanking steps. The mutated bases are underlined and in one letter code and the κB site is shown in bold.

MATERIALS AND METHODS

Sample preparation

Each strand of the 16 bp DNA duplex 5′-d($C_1T_2\mathbf{A_3}G_4G_5G_6A_7$-$C_8T_9T_{10}T_{11}C_{12}C_{13}\mathbf{T_{14}A_{15}}G_{16}$)-3′·5′-d($G_{17}A_{18}\mathbf{T_{19}}C_{20}C_{21}C_{22}$-$T_{23}G_{24}A_{25}A_{26}A_{27}G_{28}G_{29}\mathbf{T_{30}}C_{31}C_{32}$)-3′ (16M2) was synthesized on an Applied Biosystems 380B system with phosphoramidites. Deprotection was carried out with concentrated ammonia at 55°C overnight. After evaporation, the crude product was desalted on a Sephadex G-10 column eluted with 0.05 M TEAB. The eluted compound was lyophilized and subjected to two rounds of preparative HPLC. The oligonucleotide counterions were then exchanged with $NH4^+$ using a Dowex 50W-X8 $NH4^+$ column and lyophilized.

For NMR experiments, each strand was subjected to chromatography on Chelex 100 resin with sodium ions to remove divalent cations. Each single strand was dissolved in 300 µl of an aqueous buffer solution composed of 14.9 mM $MgCl_2$, 0.111 M KCl, 16 mM NaCl and 0.125 mM EDTA, pH 7. The duplex was made by mixing the two complementary strands in a 1:1 ratio, according to the calculated concentrations of each strand from the absorbance at 260 nm. The duplex was formed by incubation in a water bath at 80°C for 10 min and slow cooling. The NMR sample was obtained by lyophilizing the solution and dissolution of the resulting powder in 750 µl of 99.99% ^2H_2O. The sample was lyophilized twice to increase the percentage of ^2H_2O. The final concentration of the solution, adjusted to pH 7.0, was 2.5 mM.

NMR spectroscopy

All NMR experiments were carried out on a Varian Innova spectrometer (11.7 T) operating at a proton frequency of 500 MHz and at a phosphorus frequency of 202 MHz. The spectrometer was equipped with a 5 mm indirect detection probe. Temperatures were measured in an ethylene glycol test tube. Conformational analysis was carried out at 35 and 50°C. External DSS was used as reference for proton spectra in ^2H_2O and ^{31}P chemical shifts were calibrated with respect to external trimethylphosphate (TMP).

Proton NMR experiments. All two-dimensional proton NMR experiments were recorded in the phase-sensitive mode using the hypercomplex scheme (23). A spectral width of 5000 Hz in

both dimensions was used for proton. TOCSY (24) spectra were acquired with 2048 data points in the t_2 dimension and 512 t_1 increments. Sixteen transients were collected per increment. A homonuclear proton spin-lock with a MLEV-17 pulse sequence (25) was applied with a mixing time of 60 ms in both dimensions and the data were apodized with a shifted sine bell before Fourier transformation. NOESY (23) experiments were performed with 2048 data points in the t_2 dimension and 512 t_1 increments; 32 transients were recorded per increment. Mixing times of 50 and 300 ms were used. The data were apodized with a shifted sine bell before Fourier transformation. For the quantitative analysis of dipolar interactions, the intra-residue distance between cytosine H5 and H6 protons (2.45 Å) was used as a reference for distance calibration. The correlations that were not observed at a mixing time of 50 ms were not used to avoid possible spin diffusion artifacts. Off-resonance ROESY (26) spectra were acquired with 2048 data points and 512 t_1 increments; 64 transients were collected per increment. The experiments were performed with a 8.13 kHz effective spin-lock field generated by a series of 30° pulses over 200 ms. To avoid Hartmann–Hahn artifacts, the offset of the spin-lock carrier was moved (by 6893.8 Hz) relative to the center of the spectrum to create an angle of 54.7° between the effective spin-lock axis and the static magnetic field.

Heteronuclear ^1H-^{31}P NMR experiments. ^{31}P resonances were assigned by heteronuclear single quantum coherence selection (HSQC) using a gradient for single quantum coherence selection (27); 512 points in the t_2 dimension were acquired with 128 t_1 increments and with a spectral width of 600 Hz for phosphorous and 5000 Hz for protons. HSQC-TOCSY experiments (28) were also performed with 1024 data points, 128 t_1 increments and 256 transients per increment. A homonuclear proton spin-lock with MLEV-17 (25) was applied for a mixing time of 60 ms. The delay $\Delta/2$ was set to 17 ms for optimal polarization transfer. The data were apodized with a shifted sine bell before Fourier transformation. ^{31}P chemical shift assignments were obtained by correlation with H3′ sugar proton resonances, using proton-detected selective heteronuclear experiment SCOSYINV (selective correlated spectroscopy inverse selective pulse) with a selective pulse centered on the H3′ protons and obtained with an i-SNOB-3 180° flip angle to invert the H3′ spin population (29,30). The bandwidth covered by the soft pulse was 300 Hz, with a power level of 14 db for a pulse length of 12.74 ms. All these experiments were performed at 35 and 55°C.

Nuclear extracts

Murine pre-B cell line 70Z/3 was cultured in Glutamax-I RPMI (Gibco BRL) supplemented with 5 µg of penicillin–streptomycin, 50 µM β-mercaptoethanol and 10% fetal calf serum. We either treated 10^7 cells with 50 µg of LPS from *Salmonella abortus equi* (L-6636; Sigma) for 30 min or left them untreated. Cells were washed twice in PBS. The pellet was resuspended in 200 µl of electrophoretic mobility shift assay (EMSA) buffer I (50 mM Tris–HCl pH 7.9, 10 mM KCl, 1 mM EDTA, 0.2% Nonidet-P40, 1 mM DTT, 1 mm PMSF, 1% aprotinin, 10% glycerol). The mixture was incubated for 1 min on ice and centrifuged for 3 min at 6000 *g* at 4°C. The nuclear pellet was then resuspended in 20 µl of EMSA buffer II (20 mM HEPES pH 7.9, 400 mM NaCl, 10 mM KCl, 1 mM EDTA, 1 mM DTT, 1 mM PMSF, 1% aprotinin, 20% glycerol). The mixture was incubated on ice for 20 min and centrifuged for 10 min at 12 000 *g* and 4°C. The nuclear extracts were collected and stored at –80°C. Protein concentration was estimated using the Bio-Rad Bradford assay kit.

EMSA

Nuclear extracts were incubated with 1 µg of poly(dI–dC)·poly(dI–dC) in 20 µl of binding buffer (20 mM HEPES pH 7.5, 70 mM NaCl, 2 mM DTT, 100 µg/ml BSA, 0.01% Nonidet-P40, 4% Ficoll) for 5 min at room temperature. We added 5.4×10^5 c.p.m. of ^{32}P-labeled probe corresponding to a concentration of ~0.2 pM native NF-κB, 16M1 or 16M2 oligonucleotides and the extracts were incubated for a further 20 min. Complexes were analyzed by electrophoresis at 180 V on a 5% native polyacrylamide gel in 0.5× Tris–borate–EDTA running at 2.2 V/cm^2. The gel was dried and placed overnight in a phosphorimager. For the supershift assay, nuclear extracts were incubated for 10 min at room temperature in binding buffer in the presence of 1 µl (200 ng) of anti-p50 (1157; kindly provided by N. Israel, Institut Pasteur, Paris) or anti-p65 (sc-109; Santa Cruz) polyclonal antibody prior to addition of the probe.

RESULTS

Conformational analysis

^1H resonances were assigned by classical methods for nucleic acids (31–34). All spin systems were identified in a homonuclear TOCSY experiment and sequential assignments were obtained by homonuclear NOESY experiments with 50 and 300 ms mixing times (Fig. 2). All chemical shifts at 35 and 50°C of non-exchangeable protons, except H5′-H5" sugar protons, were unambiguously assigned. Moreover, an off-resonance ROESY experiment was used to overcome ambiguities in the assignments of H2′-H2" sugar protons as there is no spin diffusion.

The strong correlations between H6/H8 protons and H2′/H2" sugar protons observed in the NOESY experiment for a short mixing time indicated a C2′-*endo* conformation for the sugar and, therefore, B-type DNA for the duplex. The interstrand dipolar interactions between the adenine 7 H2 base proton and cytosine 27 H1′ sugar proton could be observed for the duplexes in the NOESY spectrum run at 300 ms mixing time (Fig. 2) and consequently the distances extrapolated. These interstrand distances are quite sensitive to the width of the DNA minor groove and can be used as a probe for groove geometry. For 16M2, a distance of 2.2 Å between the adenine 7 H2 base proton and cytosine 27 H1′ sugar proton was estimated, whereas the corresponding distance was ~5.9 Å for 16M1 and 3.7 Å for 16N. The minor groove would be wider for 16M1 (13) and narrower for 16M2, which might induce changes in the geometry of the major groove, in which NF-κB binds.

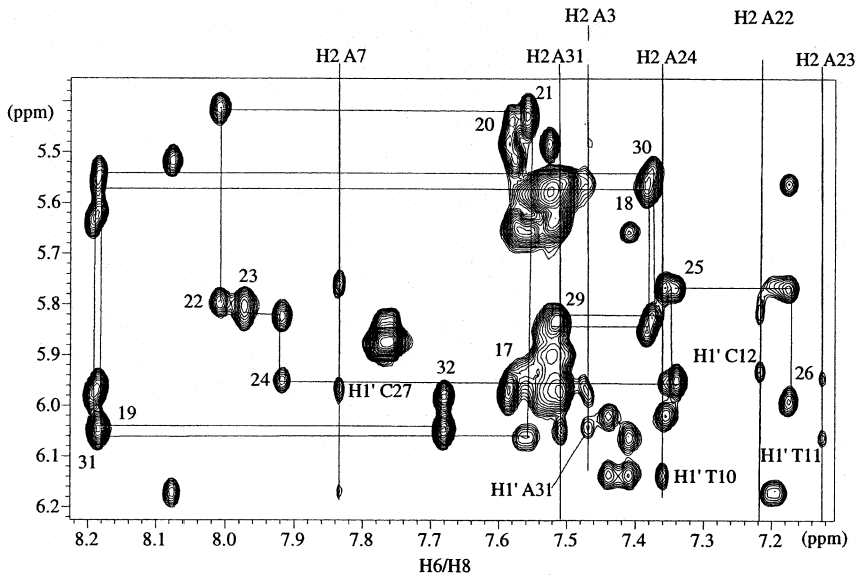

Figure 2. Correlation between the H6/H8 and H1′ protons in NOESY spectra (300 ms) at 50°C. Chemical shifts of adenine H2 protons are indicated at the top of the spectrum and interstrand NOEs between adenine H2 protons and H1′ sugar protons are annotated.

Analysis of the phosphodiester backbone

The complete assignment of ^{31}P nuclei is difficult due to the weak spectral dispersion of ^{31}P signals (Fig. 3), but is essential for determination of the conformation of the phosphodiester backbone. Indeed, ^{31}P chemical shift dispersion in nucleic acids is related to the structure, sequence and position of phosphates in the oligomer. Phosphorus resonances were assigned by HSQC spectroscopy using reverse INEPT together with TOCSY transfer (HSQC-TOCSY) and selective heteronuclear experiments, as previously described (35). As the melting point of the duplex was 67°C, these experiments were performed at both 35 and 50°C to complete the assignment of ^{31}P resonances. The limited dispersion of phosphorus chemical shifts, 0.49 p.p.m., indicates a right-handed helix for the 16M2 duplex.

Comparison of ^{31}P chemical shift dispersion for the three duplexes shows a substantially lower level of signal dispersion in 16M2 than in 16N (0.68 p.p.m.) and, to a lesser extent, in 16M1 (0.61 p.p.m.) (Fig. 4). For 16N the broad dispersal of ^{31}P signals together with the ^{31}P chemical shift behavior with temperature, as well as internucleotide H6/H8–H2" distances and the H1′ chemical shift variation with temperature (12), have been interpreted as resulting from a BI–BII equilibrium in the conformation of the phosphodiester backbone for the four κB flanking steps. The same analyses conducted for the mutated duplex 16M1 (35) was consistent with the presence of a significant BII population at steps $C_{13}pA_{14}$, $T_{19}pG_{20}$ and C_6pA_7. A small population of BII conformer may be also present in solution at the $C_{30}pA_{31}$ step. NMR results for the $C_{13}pA_{14}$ and $T_{19}pG_{20}$ steps were consistent with two BII conformers facing each other in the duplex. The limited dispersion of phosphorus chemical shifts in 16M2 suggests that the BI–BII equilibrium is displaced towards the BI conformation or is lost. This hypothesis is supported by analyses of other NMR parameters known to be important in identifying the BI–BII equilibrium, such as the lack of

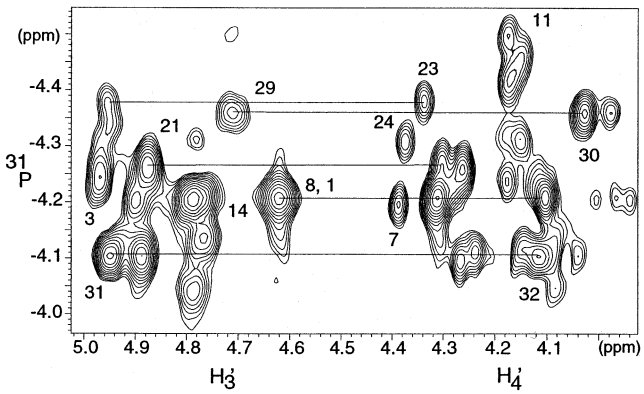

Figure 3. gHSQC experiment at 35°C showing the correlation between the H3′(i) and H4′(i + 1) sugar protons in F2 dimension and ^{31}P(i) nuclei in the F1 dimension.

downfield shifted signals for phosphorus associated with smaller NOE-derived internucleotide distances between H6/H8 and H2" sugar protons (Table 1). Thus, the NMR data showed that the backbone conformation of the 16M2 duplex differs substantially from those of 16N and 16M1. First, for the T_2pA_3 and $T_{30}pA_{31}$ steps, ^{31}P resonances are upfield shifted (chemical shifts for step 2–3 are –4.04 p.p.m. for 16N, –4.15 p.p.m. for 16M1 and –4.23 p.p.m. for 16M2; chemical shifts for step 30–31 are –3.77 p.p.m. for 16N, –4.12 p.p.m. for 16M1 and –4.17 p.p.m. for 16M2). In addition, a small internucleotide H6/H8–H2" distance, at steps T_2pA_3 and $T_{30}pA_{31}$, together with the lack of chemical shift variation upon a temperature increase, observed for the thymine H1′ (T2 and T30), imply that the BII conformer population is lost. NMR data for the $C_{13}pT_{14}$ and $A_{19}pG_{20}$ steps are consistent with a BI-only population. Indeed, ^{31}P resonances for these steps are shifted upfield (from –3.82 p.p.m. in 16N to

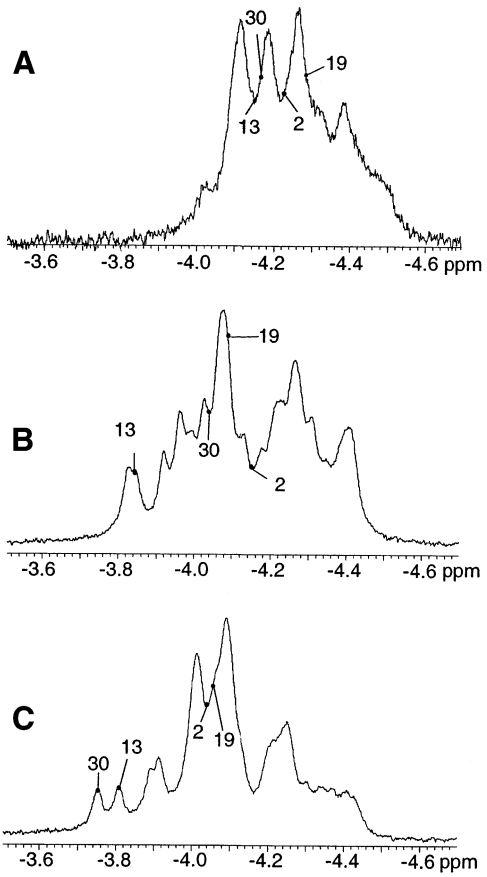

Figure 4. One-dimensional ^{31}P spectra at 35°C: (**A**) 16M2; (**B**) 16M1 and (**C**) 16N.

Table 1. NMR data for 16N, 16M1 and 16M2 indicating the conformation of the phosphodiester backbone

	16N	16M1	16M2	
^{31}P (ppm)	0.68	0.61	0.49	
$\delta_{35°C}$ ^{31}P (ppm)	-4.04	-4.15	-4.23	
$\Delta_{(50°-35°)}\delta^{31}P$ (ppm)	-0.07	0.07	-0.04	$T_{2\ P}\ G_3$
d(H6/H8-H2") (Å)	3.5	2.8	2.9	
$\delta_{35°C}H_1'$ (ppm)	5.73	5.86	5.63	$T_{2\ P}\ A_3$
$\Delta_{(50°-35°)}\delta H_1'$ (ppm)	0.1	0.03	0.01	
$\delta_{35°C}$ ^{31}P (ppm)	-3.77	-4.12	-4.17	
$\Delta_{(50°-35°)}\delta^{31}P$ (ppm)	-0.34	0.03	-0.1	$C_{30\ P}\ A_{31}$
d(H6/H8-H2") (Å)	4.0	3.1	2.9	
$\delta_{35°C}H_1'$ (ppm)	5.34	5.56	5.57	$T_{30\ P}\ A_{31}$
$\Delta_{(50°-35°)}\delta H_1'$ (ppm)	0.21	0.05	0.02	
$\delta_{35°C}$ ^{31}P (ppm)	-3.82	-3.87	-4.15	
$\Delta_{(50°-35°)}\delta^{31}P$ (ppm)	-0.09	-0.04	-0.25	$C_{13\ P}\ A_{14}$
$\delta_{35°C}H_1'$ (ppm)	5.28	5.3	5.94	$C_{13\ P}\ T_{14}$
$\Delta_{(50°-35°)}\delta H_1'$ (ppm)	0.12	0.06	-0.06	
$\delta_{35°C}$ ^{31}P (ppm)	-4.05	-4.09	-4.29	
$\Delta_{(50°-35°)}\delta^{31}P$ (ppm)	-0.05	0	-0.11	$T_{19\ P}\ G_{20}$
$\delta_{35°C}H_1'$ (ppm)	5.64	5.66	6.06	$A_{19\ P}\ G_{20}$
$\Delta_{(50°-35°)}\delta H_1'$ (ppm)	0.09	0.05	-0.04	

$\delta(^{31}P)$ is the chemical shift of phosphorus at 35°C. $\Delta_{(50°-35°)}\delta^{31}P$ is the change in phosphorus chemical shift when the temperature increases from 35 to 50°C. d(H6/H8–H2") is the internucleotide distance between the H6/H8 proton of the purine and the H2" sugar proton in the pyrimidine derived from NOE data. $\delta_{35°C}$ (H_1') is the chemical shift of the pyrimidine H1′ sugar proton. $\Delta_{(50°-35°)}\delta H_1'$ indicates changes in the H1′ sugar proton chemical shift of the pyrimidine when the temperature increased from 35 to 50°C.

–4.15 p.p.m. in 16M2 for the $C_{13}pT_{14}$ step and from –4.05 p.p.m. in 16N to –4.29 p.p.m. in 16M2 for the $A_{19}pG_{20}$ step), the H1′ resonances of the cytosine and the adenine are shifted downfield (from 5.28 p.p.m. in 16N to 5.94 p.p.m. in 16M2 for the $C_{13}pT_{14}$ step and from 5.64 p.p.m. in 16N to 6.06 p.p.m. in 16M2 for the $A_{19}pG_{20}$ step) and these H1′ resonances are shifted upfield upon a temperature increase, suggesting that the BI–BII equilibrium is displaced towards the BI conformation. Therefore, NMR data for 16M2 are consistent with a BI conformation for all steps, including the T_2pA_3, $T_{30}pA_{31}$, $C_{13}pT_{14}$ and $A_{19}pG_{20}$ steps shown to be in BI–BII equilibrium in the native duplex 16N.

Gel mobility shifts

We investigated the effect of BI–BII transition on NF-κB binding by EMSA. For the native duplex, NF-κB bound efficiently to the DNA (Fig. 5A). 16M1 clearly did not bind, whereas 16M2 binding occurred, but was less efficient than that for the native duplex, as the intensity of the band was lower under identical experimental conditions (Fig. 5A). The identity of the complex recognized by the DNA probes was confirmed by a supershift assay using antibodies against p50 or p65 NF-κB subunits. The anti-p50 antibody induced a shift of the NF-κB complex whereas the anti-p65 antibody induced its dissociation. Electrophoretic mobility shift assay and supershift assay on the three duplexes, 16N, 16M1 and 16M2, thus showed that 16M2 had an intermediate ability to bind the NF-κB heterodimer and that 16M1 did not bind.

DISCUSSION

The aim of this study was to investigate the role of the BI–BII transition in protein–DNA recognition by qualitative evaluation of the solution structure of a non-palindromic 16 bp DNA fragment related to the NF-κB-binding site. This fragment consists of the 10 bp corresponding to the native κB site interacting with NF-κB and the flanking sequences, in which 3 bp were mutated: G_3, A_{14} and G_{15} of the coding strand and C_{18}, T_{19} and C_{30} of the complementary strand were replaced by A_3, T_{13}, A_{14} and T_{18} A_{19}, T_{30}, respectively. These mutations were designed to abolish the BI–BII equilibrium observed at sequences flanking the κB site (12). The structural features of 16M2 were then compared with those observed previously for the 16 bp native sequence of the HIV-1 κB site (16N) and a mutated κB site (16M1), with a substitution at the 5′ end, within the κB site (13).

Studies of the native and mutated κB duplexes demonstrated the importance of binding site flanking sequences in terms of BI–BII transitions. For the 16N duplex, NMR data provided evidence of dynamic behavior and BI–BII

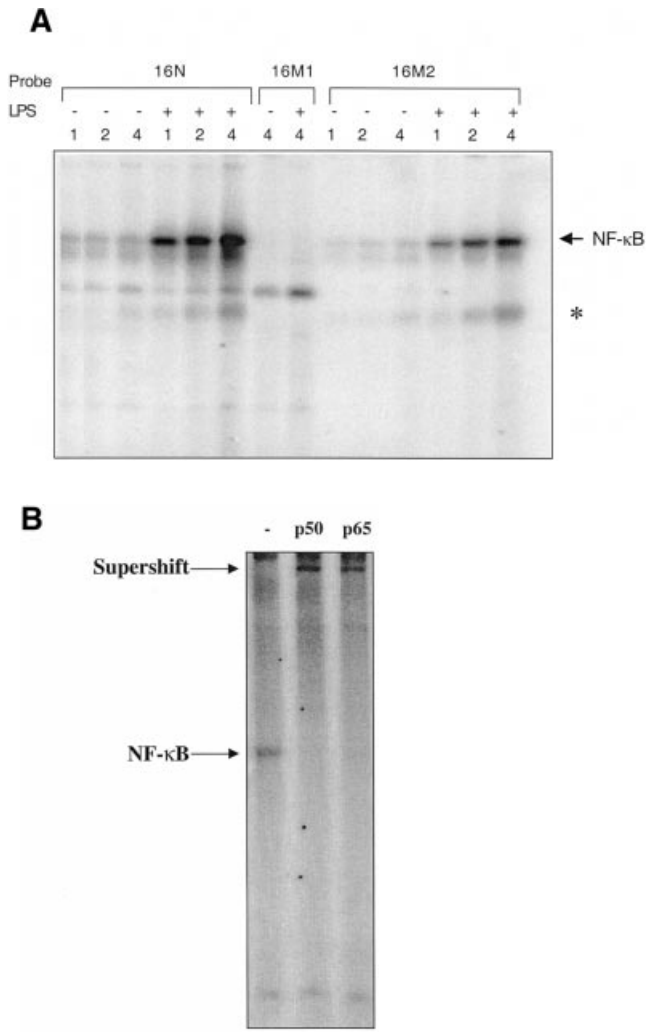

Figure 5. The M2 oligonucleotide has an intermediate ability to bind NF-κB heterodimer. (**A**) Nuclear extracts (1, 2 and 4 μg for native and mutant 2 and 4 μg for mutant 1) from cells treated or not with LPS were incubated with 5.4×10^4 c.p.m. of each NF-κB probe labeled with ^{32}P and analyzed for NF-κB binding to the probe (arrow) on a 5% native polyacrylamide gel. (**B**) Nuclear extracts were incubated in the presence of anti-p50 or anti-p65 antibody (supershift), prior to the addition of 16M2 probe, and processed as described above.

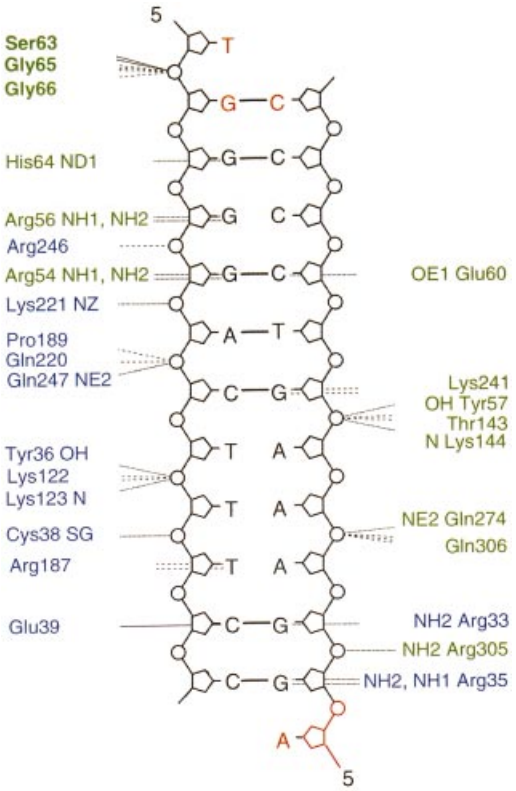

Figure 6. DNA contacts made by the heterodimer p65–p50 in the NF-κB:DNA crystal (10). Blue and green indicate the p65 and the p50 subunits, respectively. Non-bonded contacts with DNA are indicated as dashed lines and dotted lines denote hydrogen bonds to DNA. The flanking bases are represented in red and the amino acids of the protein interacting with these flanking sequences are denoted in bold.

equilibrium of the steps flanking the 10 bp binding site. In the resulting structure, the NF-κB-binding site displayed intrinsic helix axis curvature with the displacement of all κB base pairs towards the major groove. This curvature was increased by the four flanking steps being in the BII conformation. For the 16M1 BII family of structures, only a kink at the 3′ end of the duplex was observed, due to the BII conformation of two steps that faced each other, whereas at the 5′ end most of the phosphates were in the BI conformation. Therefore, 16M1 cannot mimic the conformation adopted by 16N, which is very favorable for NF-κB binding. Moreover, the smaller groove dimensions in 16M1 may hinder DNA–protein interactions. The 16M2 duplex presents all the NMR characteristics of a BI-only conformation for all the phosphates, including those previously observed to be in the BII conformation or in BI–BII equilibrium. Furthermore, 16M2 efficiently binds its target NF-κB (p50–p65), but with lower affinity than the native duplex 16N. This may be due to either loss of the BI–BII transition for the phosphates at the flanking steps and/or conformational changes of conserved bases as a result of flanking base pair mutations, inducing loss of essential DNA–protein contacts. The influence of the bases at the flanking steps is difficult to evaluate because, in most X-ray structures solved to date, the DNA fragment is the shortest possible fragment, the 10 bp of the consensus κB site (6–9). In one case, the DNA fragment was longer and included 2 bp at the 5′ end corresponding to the native sequence and a 1 bp extension at the 3′ end, different from the native sequence (10). This complex presents 36 protein–DNA contacts, only three of which concern flanking bases (Fig. 6). Gly65 and Gly66 interact with the flanking sequence, but with the phosphates rather than directly with the bases themselves (T_1pG_2 with Gly66 and Gly65 and G_2pG_3 with Gly66). Therefore, the isolated κB site may have the potential to bind efficiently due to the BI–BII equilibrium of the κB flanking sequences. However, in the X-ray structures, all the phosphates in contact with the protein are in the BI conformation; this result appears to conflict with our findings in solution. We therefore think that a BII conformation for the phosphates in sequences flanking the κB sites may be favorable and may

help to attract the protein and to bind NF-κB loops by exposing, in the major groove, accessible and polarized atoms able to establish hydrogen bonds with NF-κB. Once the complex is formed, the contacts between the protein and the DNA induce a more regular and more energetically favorable BI conformation for the phosphates of the flanking steps (13). It is interesting to note that this flexibility, already observed (13,36), occurs at TG·CA steps, which are over-represented in the consensus protein-binding site.

In this paper, we present NMR investigations and structural features of a mutated κB site with a view to elucidating the specific recognition of DNA κB sites by NF-κB. The results obtained for the native 16N duplex and the two mutated 16M1 and 16M2 duplexes stress the importance of flanking sequences for DNA–protein recognition. The dynamic behavior of the DNA phosphodiester backbone surrounding the binding site appears to play a significant role in determining specificity and conferring on the duplex, as a whole, properties that can be used by NF-κB for binding site selection. Thus, the selectivity determinants for NF-κB binding appear to depend on the deformability of an 'extended' consensus sequence. This is consistent with the hypothesis put forward by Zippora Shakked and co-workers, suggesting a structural code for DNA recognition by regulatory proteins (37,38) and based on both the intrinsic structures of DNA regions in direct contact with proteins and the deformability of DNA regions not in contact with the protein that are critical for sequence-specific protein–DNA recognition.

SUPPLEMENTARY MATERIAL

Supplementary Material is available at NAR Online.

ACKNOWLEDGEMENTS

We would like to thank Catherine Simenel for technical assistance in NMR experiments, Catherine Gouyette for the DNA synthesis and Brigitte Hartmann for stimulating discussions about the BI–BII transition. This work was supported by ECS-SIDACTION, the French anti-AIDS program.

REFERENCES

1. Nabel,G. and Baltimore,D. (1987) An inductible transcription factor activates expression of human immunodeficiency virus in T cells. *Nature*, **326**, 711–713.
2. Clark,L., Matthews,J.R. and Hay,R.T. (1990) Interaction of enhancer-binding protein EBP1 (NF-kappa B) with the human immunodeficiency virus type 1 enhancer. *J. Virol.*, **64**, 1335–1344.
3. Virelizier,J.L. (1990) Cellular activation and human immunodeficiency virus infection. *Curr. Opin. Immunol.*, **2**, 409–413.
4. Brown,K., Gerstberger,S., Carlson,L. and Franzoso,G. (1995) Control of I kappa B-alpha proteolysis by site-specific, signal-induced phosphorylation. *Science*, **267**, 1485–1488.
5. DiDonato,J.A., Mercurio,F. and Karin,L. (1995) Phosphorylation of I kappa B alpha precedes but is not sufficient for its dissociation from NF-kappa B. *Mol. Cell. Biol.*, **15**, 1302–1311.
6. Müller,C.W., Rey,F.A., Sodeoka,M., Verdine,G.L. and Harrison,S.C. (1995) Structure of the NF-kappa B p50 homodimer bound to DNA. *Nature*, **373**, 311–317.
7. Ghosh,G., van Duyne,G., Ghosh,S. and Sigler,P.B. (1995) Structure of NF-kappa B p50 homodimer bound to a kappa B site. *Nature*, **373**, 303–310.
8. Chen,Y.-Q., Ghosh,S. and Gosh,G. (1998) A novel DNA recognition mode by the NF-kappa B p65 homodimer. *Nature Struct. Biol.*, **5**, 67–73.
9. Cramer,P., Larson,C.J., Verdine,G.L. and Muller,C.W. (1997) Structure of the human NF-κB p52 homodimer-DNA complex at 2.1 Å resolution. *EMBO J.*, **16**, 7078–7090.
10. Chen,F.E., Huang,D.B., Chen,Y.-Q. and Ghosh,G. (1998) Crystal structure of p50/p65 heterodimer of transcription factor NF-kappaB bound to DNA. *Nature*, **391**, 410–413.
11. Schreck,R., Zorbas,H., Winnacker,E.L. and Baeuerle,P.A. (1990) The NF-kappa B transcription factor induces DNA bending which is modulated by its 65-kD subunit. *Nucleic Acids Res.*, **18**, 6497–6502.
12. Tisné,C., Hantz,E., Hartmann,B. and Delepierre,M. (1998) Solution structure of a non-palindromic 16 base-pair DNA related to the HIV-1 kappa B site: evidence for BI-BII equilibrium inducing a global dynamic curvature of the duplex. *J. Mol. Biol.*, **279**, 127–142.
13. Tisné,C., Hartmann,B. and Delepierre,M. (1999) NF-kappa B binding mechanism: a nuclear magnetic resonance and modeling study of a GGG→CTC mutation. *Biochemistry*, **38**, 3883–3894.
14. Lavery,R. and Sklenar,H. (1998) The definition of generalised helicoidal parameters and of axis curvature for irregular nucleic acids. *J. Biomol. Struct. Dyn.*, **6**, 63–91.
15. Lavery,R. (1998) DNA bending and curvature. In Olson,W.K., Sarma,R.H. and Sundaralingam,M. (eds), *Structure and Expression*. Adenine Press, New York, NY, Vol. 3, pp. 191–211.
16. Lavery,R. (1998) Junctions and bends in nucleic acids: a new theoretical modelling approach. In Olson,W.K., Sarma,R.H. and Sundaralingam,M. (eds), *Structure and Expression*. Adenine Press, New York, NY, Vol. 3, pp. 191–211.
17. Lavery,R., Zabrewska,K. and Sklenar,H. (1994) JUMNA (junction minimisation of nucleic acids). *Comput. Phys. Commun.*, **91**, 135–158.
18. Bertrand,H., Ha-Duong,T., Fermandjian,S. and Hartmann,B. (1998) Flexibility of the B-DNA backbone: effects of local and neighbouring sequences on pyrimidine-purine steps. *Nucleic Acids Res.*, **26**, 1261–1267.
19. Hartmann,B., Piazzola,D. and Lavery,R. (1993) BI–BII transitions in B-DNA. *Nucleic Acids Res.*, **11**, 561–568.
20. Schroeder,S.A., Roongta,V., Fu,J.-M., Jones,C.R. and Gorenstein,D.G. (1989) Sequence-dependent variations in the ^{31}P NMR spectra and backbone torsional angles of wild-type and mutant Lac operator fragments. *Biochemistry*, **28**, 8292–8303.
21. Lefebvre,A., Mauffret,O., Hartmann,B. Lescot,E. and Fermandjian,S. (1995) Structural behaviour of the CpG step in two related oligonucleotides reflects its malleability in solution. *Biochemistry*, **34**, 12019–12028.
22. Gorenstein,D.G., Schroeder,S.A., Fu,J.M., Metz,J.T., Roongta,V. and Jones,C.R. (1988) Assignments of ^{31}P NMR resonances in oligodeoxyribonucleotides: origin of sequence-specific variations in the deoxyribose phosphate backbone conformation and the ^{31}P chemical shifts of double-helical nucleic acids. *Biochemistry*, **27**, 7223–7237.
23. States,D.J., Haberkorn,R.A. and Ruben,D.J. (1982) A two-dimensional nuclear Overhauser experiment with pure absorption phase in four quadrants. *J. Magn. Reson.*, **48**, 286.
24. Greisinger,C., Otting,G., Wüthrich,K. and Ernst,R.R. (1988) Clean TOCSY for ^{1}H spin system identification in macromolecules. *J. Am. Chem. Soc.*, **110**, 7870.
25. Bax,A. and Davis,D.G. (1985) MLEV-17-based two-dimensional homonuclear magnetization transfer spectroscopy. *J. Magn. Reson.*, **65**, 355–360.
26. Desvaux,H., Berthault,P., Birlirakis,N., Goldman,M. and Piotto,M. (1995) Improved version of dynamic ROESY. *J. Magn. Reson.*, **113**, 47–52.
27. Wilker,W., Leibfritz,D., Kerssebaum,R. and Bermel,W. (1993) Gradient selection in inverse heteronuclear correlation spectroscopy. *Magn. Reson. Chem.*, **31**, 287–292.
28. Norwood,T.J., Boyd,J. Heritage,J.E., Soffe,N. and Campbell,I.D. (1990) Comparison of techniques for ^{1}H-detected heteronuclear ^{1}H-15N spectroscopy. *J. Magn. Reson.*, **87**, 488–501.
29. Sklenàr,V. and Bax,A. (1987) Measurement of ^{1}H-^{31}P coupling constants in double-stranded DNA fragments. *J. Am. Chem. Soc.*, **25**, 7525–7526.
30. Kupce,E. and Freeman,R. (1995) Short selective pulses for biochemical applications. *J. Magn. Reson.*, **112**, 134–137.
31. Clore,G. and Gronenborn,A.M. (1985) Probing the three-dimensional structures of DNA and RNA oligonucleotides in solution by nuclear Overhauser enhancement measurements. *FEBS Lett.*, **179**, 187–198.
32. Wüthrich,K. (1986) *NMR of Proteins and Nucleic Acids*. John Wiley & Sons, New York, NY.

33. Van de Ven,F.J.M. and Hilbers,C.W. (1988) Resonance assignments of non-exchangeable protons in B type DNA oligomers, an overview. *Nucleic Acids Res.*, **16**, 5713–5720.
34. Wijmenga,S.S., Mooren,M.M.W. and Hilbers,C.W. (1993) NMR of nucleic acids; from spectrum to structure. In *NMR in Macromolecules: A Practical Approach*, Oxford University Press, Oxford, UK, pp. 217–288.
35. Tisné,C., Simenel,C., Hantz,E., Shaeffer,A. and Delepierre,M. (1996) Backbone conformational study of a non-palindromic 16 base pair DNA duplex exploring 2D 31P-1H heteronuclear inverse spectroscopy: assignment of all NMR phosphorus resonances and measurement of $^{3}J^{31}P\text{-}^{1}H_{3}'$ coupling constant. *Magn. Reson. Chem.*, **34**, 115–124.
36. Weisz,K., Shafer,RH., Egan,W. and James,T.L. (1994) Solution structure of the octamer motif in immunoglobulin genes via restrained molecular dynamics calculations. *Biochemistry*, **11**, 354–366.
37. Rozenberg,H., Rabinovich,D., Frolow,F., Hegde,R.S. and Shakked,Z. (1988) Structural code for DNA recognition revealed in crystal structures of papillomavirus E2-DNA targets. *Proc. Natl Acad. Sci. USA*, **95**, 15194–15199.
38. Hizver,J., Rozenberg,H., Frolow,F., Rabinovich,D. and Shakked,Z. (2001) DNA bending by an adenine-thymine tract and its role in gene regulation. *Proc. Natl Acad. Sci. USA*, **98**, 8490–8495.